Langmuir

Article

pubs.acs.org/Langmuir

Spreading of a Suspension Drop on a Horizontal Surface

Jeongin Han and Chongyoup Kim*

Department of Chemical and Biological Engineering, Korea University, Anam-dong, Sungbuk-ku, Seoul 136-713, Korea

Supporting Information

ABSTRACT: Experimental studies were performed on the contact line motion of a suspension of PS particles on a glass surface. The base liquids were silicone oil and glycerin. The particle size was in the range of 1−6 μm and the particle loading was 0.5−5 vol %. The drop shape was determined by using a drop image and its reflection and the drop outline was traced to the subpixel level. The Tanner−Voinov−Hoffman relation was valid for suspensions as well as for pure liquids. Silicone oil suspensions showed almost no noticeable change compared with the pure fluid. Glycerin suspensions showed an increase in contact line speed at low particle loading. The difference was due to the microstructure change at the contact line region, and the microstructure change was originated from the wetting characteristics of particles. Particle alignment occurred during the spreading stage for partially wetting particles. The contact line showed a stop-and-go fashioned motion due to surface irregularities. This result can be used as the boundary condition at the contact line in the numerical simulation of suspension spreading.

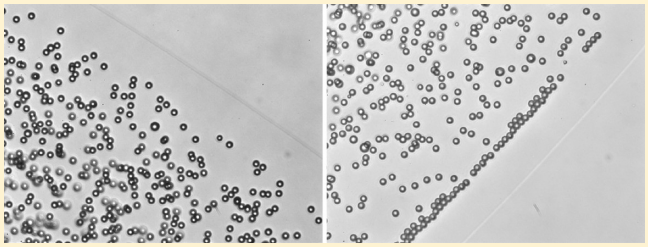

INTRODUCTION

The spreading of liquid on a solid surface is important in many industrial processes such as inkjet printing,[1,2] coating,[3−5] and pesticide deposition.[6,7] The spreading is also important in biology[8] and human eyes.[9] In the spreading of a liquid, a contact line arises at the intersection of the liquid, a gas, or another liquid and a solid. At the equilibrium the tangent drawn at the contact line to the liquid−gas interface forms an "equilibrium contact angle" with respect to the solid surface. The equilibrium contact angle varies depending on wettability. At the dynamic state, the measured angle formed at the contact line is not the same as the equilibrium contact angle, and the contact line moves toward the equilibrium state. Reflecting its importance, the contact line problem has been reviewed frequently.[8,10−14] Recently, a comprehensive review on wetting and spreading was given by Bonn et al.,[8] and hence, it is not repeated here. Until now, the contact line problem has been focused on homogeneous liquids except for the case of nanoparticle suspensions.[15−21] In printing and coating, suspensions are spread on solid substrates. Especially in the case of electrode coating of secondary cells, the particle size in the slurry has an order of a few micrometers. Therefore, it should be of practical importance to study the motion of the contact line of suspensions of micrometer-sized particles. In the case of micrometer-sized particles, the effect of colloidal force and disjoining pressure[15−17] that appear at a smaller length scale can be excluded, and hence, the hydrodynamic and interfacial effects can be investigated separately in the contact line motion of suspensions of any particle sizes.

It has been known that the stress at a contact line diverges when the classical no-slip boundary condition is used at the solid boundary;[22] hence, the hydrodynamic theory fails. To remedy the problem, the slip boundary condition has been introduced[23] with a slip length. But the slip length is still an unknown parameter, and the theory may not represent the physics at the contact line correctly. De Gennes[11] noticed the existence of precursor film in front of the contact line and estimated the length of the film to be on the nanometer order. Recently, Hoang and Kavehpour[24] measured the time evolution of the precursor film focusing on the inflection point in the drop surface profile and showed that the values were in good agreement with the theoretical predictions in which the length would be proportional to the square root of time. Using a slip boundary condition at the solid−liquid interface, Hocking[25] analyzed the spreading of a drop on a solid surface at low and high Bond number. At low Bond numbers, by using the lubrication approximation, he derived a governing equation on the drop surface profile and solved the equation by the matched asymptotic expansion. He found that, in addition to the usual inner and outer regions, an intermediate region had to be placed between the inner and outer regions to properly match the inner and outer solutions. Physically it is known that the contact line region can be divided into three regions:[8] The inner region is a liquid film of a few nanometers where molecular level analysis is required. The intermediate region is the contact line region where an inflection point appears in the surface profile due to the balance of viscous and capillary forces. The length of the intermediate region has a size of 3Ca R/θ_c, where Ca = $\mu U/\sigma$ is the capillary number and μ is viscosity, U is the contact line velocity, σ is surface tension of the liquid, and θ_c is the contact angle. The outer region is the macroscopic region where the gravity and surface forces are balanced. Here it

Received: October 31, 2011
Revised: December 24, 2011
Published: January 3, 2012

   dx.doi.org/10.1021/la204256z | *Langmuir* 2012, 28, 2680−2689

is noted that the size of the intermediate region has an order of micrometers for a typical drop spreading problem. This means that, in the case of suspensions, particles contained in the intermediate region can strongly affect the drop surface profile and hence contact line motion. Voinov[26] approached the contact line problem without considering the inner region while introducing a cutoff length scale, h_m, and the angle at the position, θ_m. He showed that the dynamic angle θ at the position with surface height h and the following relation with capillary number, Ca:

$$\theta^3 - \theta_m{}^3 = 9\mathrm{Ca}\ln(h/h_m), \quad \theta < 3\pi/4 \tag{1}$$

Tanner[27] solved the Stokes equation near the contact line and showed that the tangent, hence the angle at the inflection point of the drop profile, had the similar relation to the above Voinov result. He also derived scaling laws on drop radius vs time in power-law of time. Hoffman's data[28] support the Voinov's and Tanner's theoretical derivations. Hence, combining Voinov's and Tanner's derivations gave the following Tanner–Voinov–Hoffman (TVH) relation, which has been widely used

$$\mathrm{Ca} = \kappa(\theta^3 - \theta_m{}^3) \tag{2}$$

where the logarithmic term in eq 1 has been replaced by a constant κ, which is found to be approximately 0.013 when Hoffman's data on silicone oils are used.

As described already, in the case of suspensions, the contact line dynamics can be altered from the pure liquid case and it will manifest itself by the change in κ or even the functional form of the TVH relation. Also changes in the microstructure of particles may occur from the random distribution in the bulk state near the contact line, which may also affect the contact line dynamics. Recently, Sangani et al.[29] analyzed the capillary and hydrodynamic forces experienced by particles that protruded from the drop surface near the contact line to derive the condition for pinning of the contact line in drying of a suspension drop. Also they observed the motion of the particles near the contact line experimentally. They have reported that particles move toward the contact line by the radially outward flow due to drying and the surface tension exerts forces on the particles captured along the contact line toward the center of the drop. Hence, depending on the relative magnitude of hydrodynamic and surface tension forces, particles can move outward or inward, and hence, the contact line pinning characteristics can be changed. Even though the physical situation may not be the same, since the contact line is moving outward in the present case while the contact line is pinned or moving inward in the case of drying, we note that the force acting on particles captured at the contact line region should be qualitatively the same, and the particles are expected to play a role in the contact line dynamics of suspension.

In the present research we have investigated the effect of dispersed particles on the motion of the contact line. In doing so, we have considered only the hydrodynamic effect by adding no surfactant, polymer, or electrolyte, which is usually added for better dispersion of particles. Also, since the minimum particle diameter is 1 μm, van der Waals force between particles is considered to be small, and therefore, the hydrodynamic effect is assumed to be dominant together with the surface tension effect.

EXPERIMENTAL SECTION

Materials. As the base liquid, silicone oil (KF96, Shinetsu Chem. Co.) or glycerin (Junsei Chem. Co., GR grade) was used. The average molecular weight and the polydispersity of the silicone oil are 25 000 Da and 2.0, respectively, according to the manufacturer's specification. Both of the fluids have shear-independent viscosity. In Table 1, the viscosity and surface tension of the liquids are listed. As the suspending particle polystyrene (PS) particles of 1, 2, 3.5, and 6 μm were used. The PS particles were polymerized by the dispersion polymerization method.[30,31] This range of particle size was chosen so that the particle size and the length scale of the intermediate region are comparable. Particle loading was changed from 0.5 to 5 vol %. The particle size distributions were found to be virtually monodisperse as shown in Figure 1. As the surface for spreading experiments, slide glasses were used. In order to remove both organic and inorganic contaminants on the slide glass, the piranha etch method was used. To do so we first diluted the cleaning solution (Micro 90, Aldrich) to 2% in water. Slide glasses were immersed in the diluted cleaning solution, and the solution was stirred by a magnetic stirrer for 60 min. Then the slide glasses were cleaned by ethanol several times and then purged by nitrogen gas. Hydrogen peroxide solution (30%) and sulfuric acid (95–98%) were mixed in a jar so that the volume % of sulfuric acid was 75% by adding sulfuric acid slowly. During the preparation of the piranha solution bubbles formed. After the bubbles disappeared the slide glasses were immersed in the glass jar and the jar was placed on a hot plate of 100 °C for 15 min. Finally, the slide glasses were rinsed by ultrapure water generated by a Millipore water system and purged with nitrogen gas. In Figure 2, the AFM image of the cleaned solid surface is shown. Some defects can be seen and the average distance between the neighboring defects was on the order of a few hundred nanometers. Also the height of the defect is 1–10 nm and its rms (root-mean-square) value is 1.4–1.9 nm. It has been reported that the roughness of this size does not affect the advancing contact angle or drop spreading.[32,33]

Table 1. Viscosity and Surface Tension of the Liquids at 24 °C

	viscosity (mPa s)	surface tension (mN/m)
water	0.914	72.2
glycerin	891.9	64.1
silicone oil	970.0	21.2

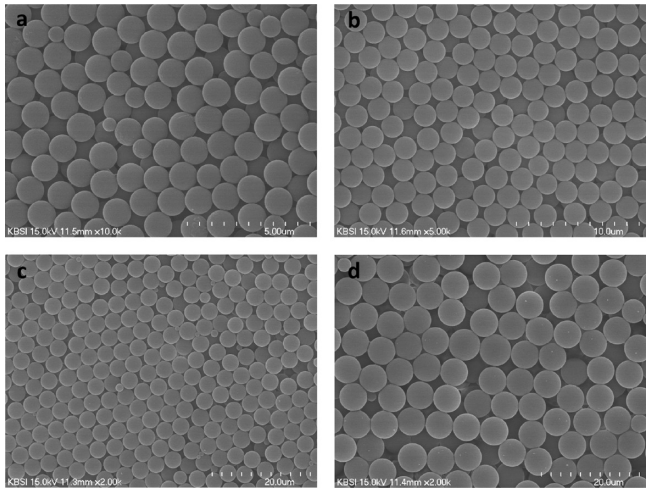

Figure 1. SEM images of particles: (a) 1 μm, (b) 2 μm, (c) 3.5 μm, and (d) 6 μm.

Drop Generation. A drop of liquid sample was squeezed out of a syringe tip (21 gauge, nozzle diameter of 510 μm) by using a commercial dispenser (EFD Ultimus) which is operated by pressurized air and a vacuum with a preset sequence of pressure profiles. The amount of liquid drop at each run was 3.5 μL for silicone oil (drop diameter 1.9 mm) and 8 μL for glycerin (drop diameter 2.5 mm).

dx.doi.org/10.1021/la204256z | Langmuir 2012, 28, 2680–2689

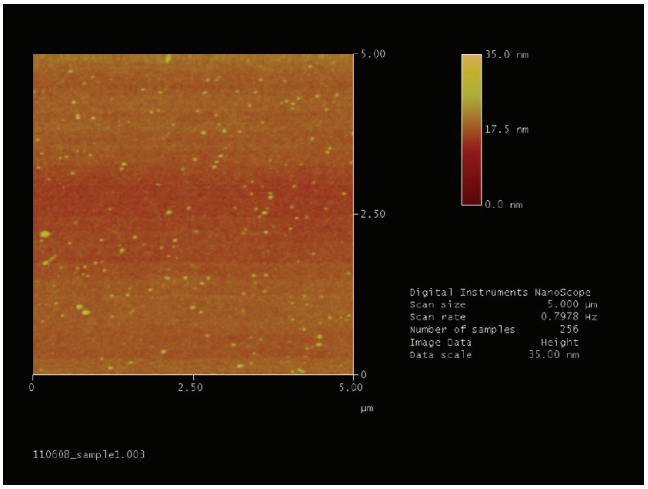

Figure 2. AFM image of the cleaned solid surface.

The difference in diameter is due to the difference in surface tension. The drop volume of a pure liquid was virtually the same as the drop volume of suspension made from the same liquid. The syringe was installed on a motorized $x-z$ stage and the syringe tip was positioned so that the axis of the tip was coaxial to the microscope objective lens when the liquid was being dispensed. The distance between the slide glass surface and the syringe tip was kept at the same distance for reproducibility. To do this the zero position was set before all the experimental runs and the syringe was moved to the desired position by the motorized stage. All the experiments were performed in an air-conditioned room at 24 °C. Even though the temperature variation was nominally ±1 °C, the actual variation was less than 0.75 °C. All the materials and equipment were stored at room temperature, and hence, the temperature of the liquid should be virtually the same as the slide glass temperature and there should be no heat transfer effect during spreading.

Imaging of Drop. To observe the movement of contact line at the edge of a drop spreading on a slide glass placed on an inverted microscope (Olympus IX51) we took images from the side of the drop at a prescribed time interval of $^1/_{500}$ s. The whole system was installed on an optical table to minimize the vibration from the environment. When taking images from the side, a CMOS camera (Mikrotron EoSENSE MC1362) and a Nikon lens (50 mm normal lens) and extension tubes were used. The exact specification on the depth of field of the lens of the optical system is not available from the manufacturer, since two extension tubes were installed on the original Nikon lens for the best close-up view. It was found to be approximately 100 μm when the distance between the drop edge and the lens is 7.4 cm. For illumination of the drop, an LED light source (Schott LLS, 15 W) and a backlight guide (Schott, Single 51 × 51 backlight A08920) were to avoid heating up the sample or the slide glass. Even though the slide glass was placed on the microscope, the movement of contact line could not be observed from below and from the side simultaneously, since the microscope window was so narrow while the contact line speed was too fast; hence, the contact line came out of view in 1 s. Therefore, the image from below was taken while moving the slide glass manually only to observe the microstructure of particles near the contact line and the relative position for a short time. To take the image from below, a CCD camera (Imperx 2M30L) was used. The images were captured with a rate of 500 frames per second.

Image Processing. To obtain the contact angle and contact line speed from the images taken at the same time interval, the drop shape was determined by using an image processing technique. In Figure 3a, a typical image of a drop is shown. When we took the image from the side, the image reflected by the slide glass was also taken. In this case the drop diameter at the foot is 4.38 mm and the pixel size is 20.8 μm. Then we can detect the edge of the drop by using the Sobel method[34] in Matlab software, as shown in Figure 3b, as a white line over the black background. A more accurate drop outline was obtained by the following method. Since the Sobel method gives only the digitized data, the movement of contact line will look like a stop-and-go type except at the initial stage of movement. Also, since the pixel size is 20.8 μm in the present experiment and the maximum resolution is limited by the pixel size with this method, the drop outline is not accurate enough to determine the position of the contact line accurately and, more importantly, the contact angle accurately, since it is very sensitive to the shape of the drop near the contact line. When the gray values near the drop edge are examined, it is difficult to locate the edge exactly as shown in Figure 3c. Here we assume that the exact drop edge should be located at the position where the gray value is 128. (The most bright gray value is 255, while the complete darkness corresponds to 0 in 8 bits per pixel image.) Then, for each column in the image, by finding the pixel at which the gray value is near 128 and its neighboring pixel values, the subpixel position at which the gray value should be 128 is determined by the linear interpolation of gray values of the neighboring pixels. We detected both the real and mirror images of the drop near the contact line. To determine the contact line

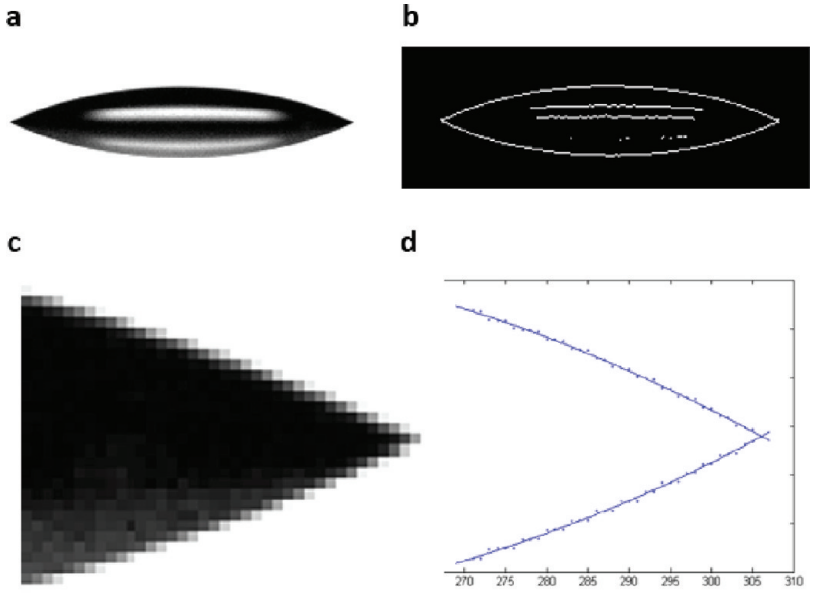

Figure 3. (a) Typical drop image, (b) Sobel outline, (c) drop edge, and (d) contact line position determination.

dx.doi.org/10.1021/la204256z | *Langmuir* 2012, 28, 2680−2689

position and contact angle accurately we fit 35 points near the contact line to a third-order polynomial and generated two curves, one from the real image and the other from the reflected image. We have found that a more robust position can be obtained when we fit the drop shape without using the first pixel near the apparent contact point, since the contact angle is measured from the macroscopic drop profile.[8] The contact line position is set to be the intersection of two curves, as shown in Figure 3d. The advancing contact angle is calculated at the intersection. To determine the local velocity of the contact line five consecutive images were fitted to a linear equation and then the derivative was calculated at the middle image.

RESULTS AND DISCUSSION

Before describing the experimental results, some possible errors due to room temperature variation are considered. To check whether there could be a significant change in contact angle or contact line position due to change in refractive index (RI) of the liquid when the temperature fluctuates, we tested the temperature effect by using a solid sample that does not change shape with temperature. To do so we made a solid PS drop of a truncated-sphere shape on a slide glass by melting a PS pellet and solidifying it. After the solidification, the shape could be assumed to be the same regardless of temperature. Then we took images of the solid PS while changing the temperature of the PS sample on a heated surface (a temperature controlled ITO surface) between 23 and 42 °C. Then the RI of PS[35] changes by 0.002 47, which is about 4 times larger than the possible variations in RI of glycerin[36] (0.0005) or silicone oil[37] (0.000 66) due to the maximum room temperature variation of 2 °C. It was found that the change in contact line position and contact angle remained within 25 μm and 0.4° between 23 and 42 °C, respectively, for the PS solid. Therefore, the change in contact line position and contact angle for the liquid cases should remain below 6 μm and 0.1°, respectively, due to refractive index change and can considered to be negligibly small. The temperature variation also can change the viscosity and surface tension of fluid, which can result in the change in contact line velocity. For glycerin, the change in viscosity is 6%, while the change in surface tension is 0.1% when the room temperature varied ±1 °C. However, this variation does not seem to affect the value of κ because of the following reason. When the viscosity of fluid becomes smaller, the velocity will become faster. Since the flow is Stokes flow, the change in velocity will be inversely proportional to viscosity. Since the surface tension is almost constant, the driving force will be the same and therefore the capillary number will not be changed and hence the value of κ. Hence, the temperature variation does not seem to cause any significant error in the final result under the experimental conditions.

Another possible source of error is ill-focusing. Since the drop was positioned at the same position and the drop spread radially on a clean surface, well-focused images should be obtained theoretically. However, there could be a problem when the drop is out of focus in a certain degree due to deviation from the perfectly radial spreading on an irregular surface. To check for this problem, images were taken while changing the distance between the objective lens and the solid drop, and the contact angle and position were calculated. It was found that the angle remained within 2° when the lens moved 0.5 mm from the focal length. In our case, the depth of focus is 100 μm, and hence, the variation in contact angle will be 0.4°. This value is far smaller than the usual variation in contact angle, and hence, ill-focusing cannot cause a meaningful error.

In Figure 4, the variations of drop radius with time are plotted for the silicone oil and glycerin and two of their

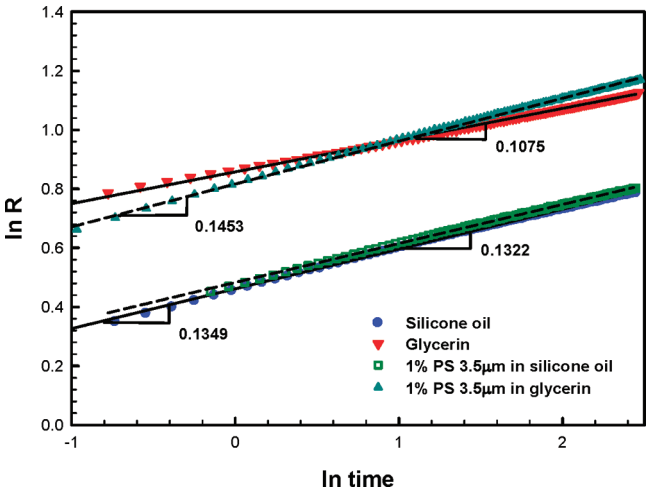

Figure 4. ln $R(t)$ vs ln t for pure liquids and their suspensions of 3.5 μm spherical particles.

suspensions. For all cases, ln $R(t)$ vs ln t show linear relations or power law of $R(t) \propto t^{1/n}$, confirming that the Tanner's law[27] is satisfied for both pure liquids and their suspensions. However, the n values are different. In the case of pure glycerin, n is 9.30, which is quite close to 10 for viscous and surface tension driven motions.[38] In the case of pure silicone oil, n is 7.41, which is close to 7 for gravity and surface tension driven motions.[39] Considering that the capillary lengths of the silicone oil and glycerin are 1.47 and 2.56 mm while the drop diameters of silicone oil and glycerin are 1.9 and 2.5 mm, respectively, the viscosity driven characteristic for glycerin and the gravity driven characteristic for the silicone oil appear to be reasonable. In the case of the suspension in silicone oil, the n value 7.56 is virtually the same as the pure liquid value, while the n = 6.88 of the suspension of glycerin is qualitatively different from the pure liquid value. This does not mean that the contact line motion of the glycerin suspension becomes gravity driven, since the viscosity remains the same. The faster movement of the suspension should be caused by a different driving mechanism, which will be considered later. In any case, the drop spreading should be driven by the contact line motion.

Next we checked whether the Tanner–Voinov–Hoffman (TVH) relation should be applied to our case from a different approach. In Figure 5, a typical relation between Ca (capillary number) and θ^3 is shown for the silicone oil and a suspension of 3.5 μm particles in the silicone oil. From the linear relationships it can be confirmed that the TVH relation (eq 2) is valid for both the pure fluid and the suspension. It is also noted that the fitted slope value of 0.012 is sufficiently close to the value of 0.013 extracted from the Hoffman's data and Shiaffino and Sonin's derivation.[40] In this case, the intercept at the vanishing contact line speed also vanishes, meaning that the equilibrium contact angle is 0°. In Figure 5 the experimental data points become more scattered as Ca becomes smaller, in other words, as time elapses. When the data were plotted without the scattered data below Ca of 0.0025, the slope value of 0.012 did not change. This means that the TVH relation is valid through the later stage of spreading, even though there is scattering. The issue of data scattering at the final stage of

dx.doi.org/10.1021/la204256z | Langmuir 2012, 28, 2680–2689

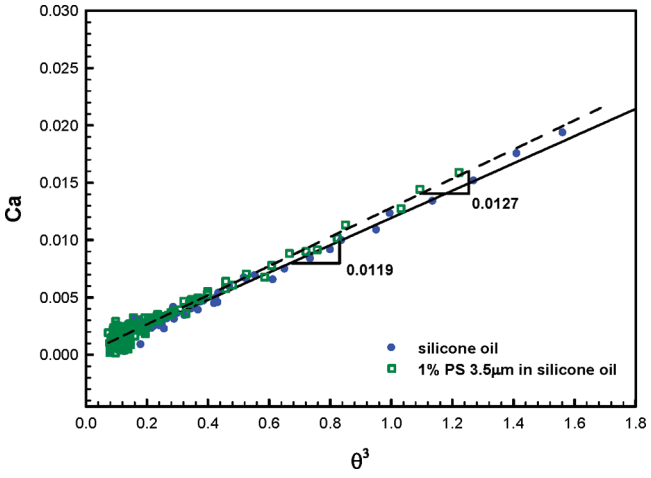

Figure 5. Ca vs θ^3 for silicone oil and its suspension.

spreading will be considered in the later part. From the match between the literature value and the present experiment with the silicone oil, the equipment and data processing methods used in the present research are considered to be validated.

In Figure 6, the variations of Ca are plotted as a function of θ^3 for glycerin and the suspensions of 3.5 μm particles in

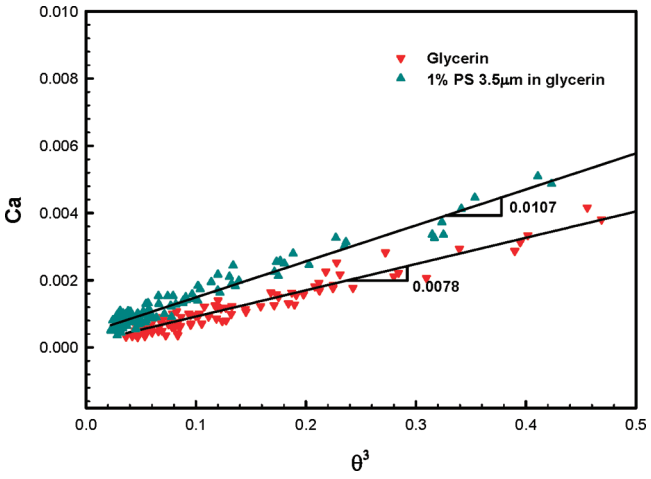

Figure 6. Ca vs θ^3 for glycerin and its suspension.

glycerin. Both cases show that the TVH relation is valid regardless of the presence of particles, but with different slopes. Also the equilibrium contact angle for each case is 0°, as in the case of the pure silicone oil. The presence of particles changes the contact angle slightly from the pure liquid value in this case. Here Ca's of suspensions of particle loading of 1 vol % (% hereafter) are calculated on the basis of the pure liquid viscosity rather than the suspension viscosity. In the case of pure silicone oil and the suspension in silicone oil, the κ's are almost the same. This means that the speed of moving the contact line of the suspension is virtually the same as that of silicone oil without particles, since the viscosity of the dilute suspension is almost the same as the pure liquid. In the case of glycerin, however, the speed of the moving contact line of the suspension is slightly faster than that of pure glycerin.

Figures 7 and 8 show the effect of particle concentration on the change in spreading characteristics. Each data point was obtained by averaging at least four independent experiments. In the case of silicone oil, κ's are almost constant, regardless of particle loading, except that the κ's when $\phi = 0.05$ appear to be slightly smaller than the κ's at lower particle loadings. In other words, the presence of particles does not affect the speed of the moving contact line within the range of particle loading considered here. In the case of glycerin suspension, however, κ's increase first with particle loading and then decrease in such a way that the κ's when $\phi = 0.05$ are almost the same as the value when there is no dispersed particle. The particle loading for the maximum κ is not the same, and there is a tendency for the particle loading at the maximum κ to shift to more dilute particle concentration, except for the case of 1 μm particles. Due to the large deviation in κ values, the particle loading that gives the maximum κ may not be statistically significant. The reason for the change in κ depending on particle loading will be considered in the later part of the present paper after considering the microstructure of particles near contact line.

Figure 9a–d shows the distribution of particles near the moving contact line for the case of silicone oil base suspensions. Regardless of particle size and particle loading, particles are randomly distributed near the contact line as well as in the bulk state. It is noted that particles are located away from the contact line, and in the case of 5% suspensions, there is a discernible edge of the particle-free region. However, particles are randomly distributed along the edge, even if the approximate edge can be recognized. When the contact line region is examined under a microscope, some particles approach the contact line, turn around, and then move back to the bulk region (Supporting Information, video 1). Only a small number of particles stay near the contact line. In the case of glycerin base suspensions, as shown in Figure 9e–h, the distribution of particles is quite different at the edge from silicone oil base suspensions while it is random in the bulk: Particles are chained at the edge from the early stage of spreading and they become hexagonally packed at the edge region when the number of particles is large. Near the contact line it was observed under the microscope that particles moved to the end of the chained particles one by one while moving toward the contact line (Supporting Information, video 2). The chaining process continued until the chain almost filled the edge line. It is certain that the arrangement of particles near the contact line should affect the contact line dynamics.

When a suspension drop is spread on a solid surface, a particle-free band appears between the bulk region and the three-phase contact line, as shown in Figure 9. The length of the particle-free region increases with time in a logarithmic fashion for all the suspensions in silicone oil and glycerin, as shown in Figure 10. In the case of the suspension in silicone oil, the length increases indefinitely. In this case, the contact angle approaches the equilibrium contact angle of pure silicone oil on the slide glass. However, in the case of suspension of large particles, say 6 μm, in glycerin, the length increases to a certain point and then the contact line begins to recede. The receding of the contact line continues until an equilibrium state is reached, and the contact angle does not appear to be the same as the value for pure glycerin without particles. When receding occurs, the TVH relation should no longer be valid and it has to be regarded as a new regime, which appears only in the case of some suspensions of large particles. Sangani et al.[29] have reported that the receding occurs when the surface tension force exerted on the protruded particles near the contact line exceeds the hydrodynamic force acting on the particles due to drying. The increase of the particle-free region is caused by the

dx.doi.org/10.1021/la204256z | Langmuir 2012, 28, 2680–2689

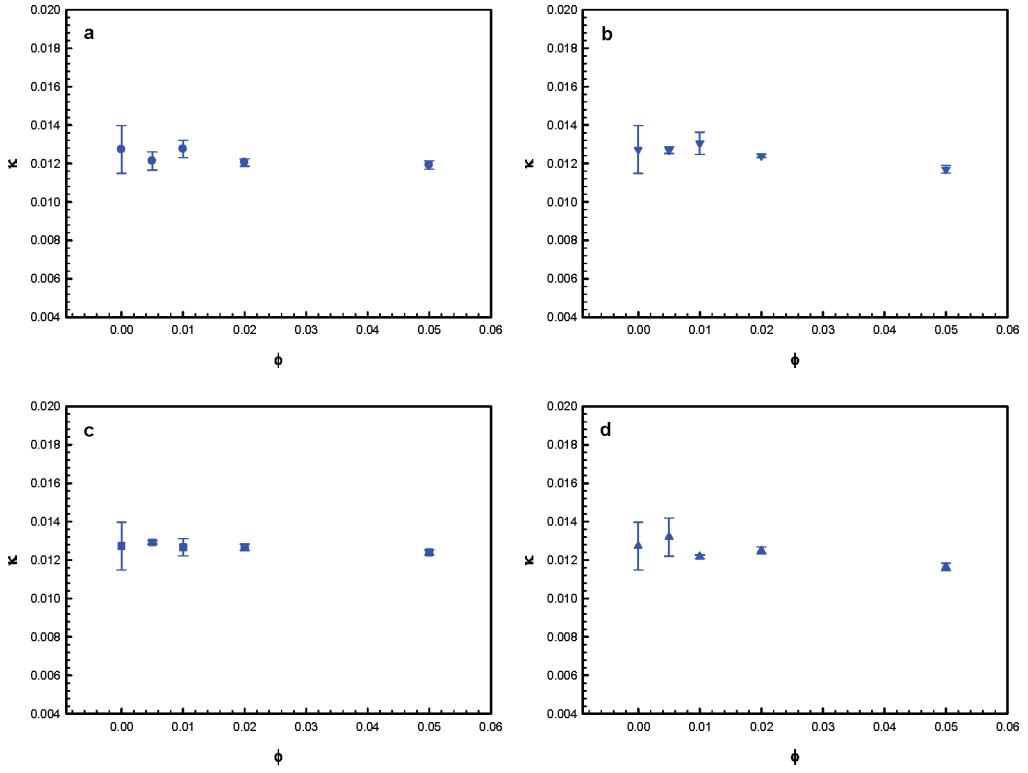

Figure 7. κ vs particle concentration for suspensions of different particle sizes in silicone oil: (a) 1 μm, (b) 2 μm, (c) 3.5 μm, (d) 6 μm.

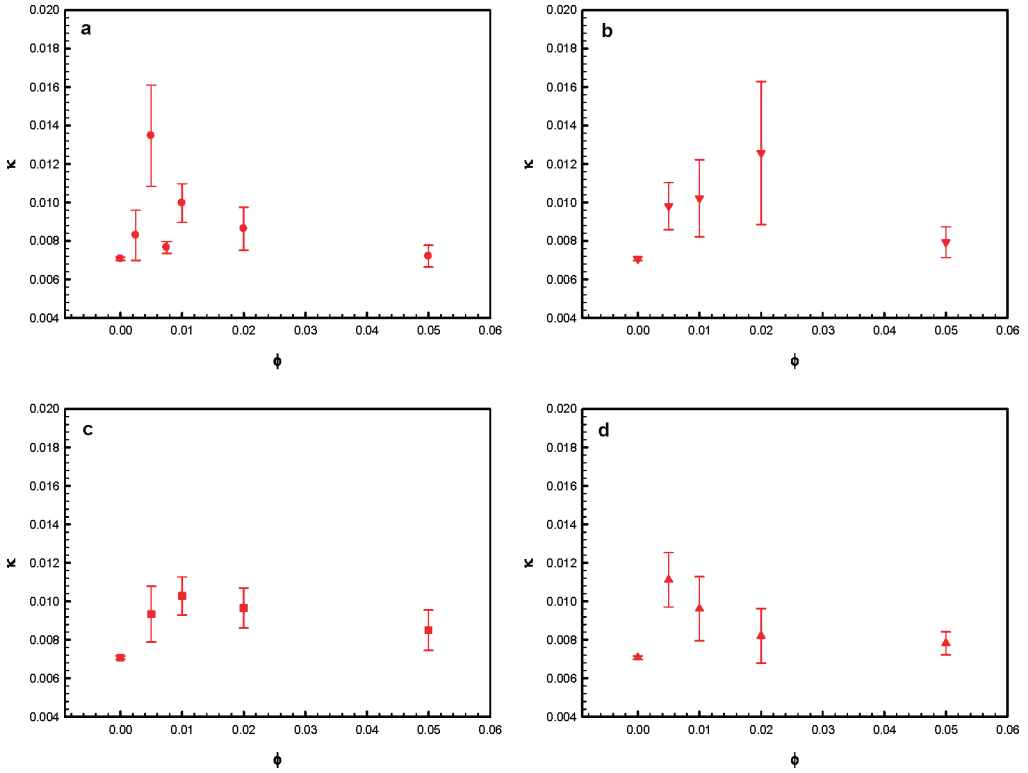

Figure 8. κ vs particle concentration for suspensions of different particle sizes in glycerin: (a) 1 μm, (b) 2 μm, (c) 3.5 μm, (d) 6 μm.

drainage of fluid through the interstices formed by two adjacent particles and the solid surface. The drainage is caused by the capillary motion of the contact line and by this motion there is a continuous, radially outward flow to the moving contact line from the bulk region. The flow should be relatively strong at the early stage due to a strong capillary force at the contact line (the dynamic contact angle is large) and the alignment is set in at this stage.

We now consider, on the basis of the microstructure formation, why the contact line speed of suspension in glycerin

dx.doi.org/10.1021/la204256z | *Langmuir* 2012, 28, 2680−2689

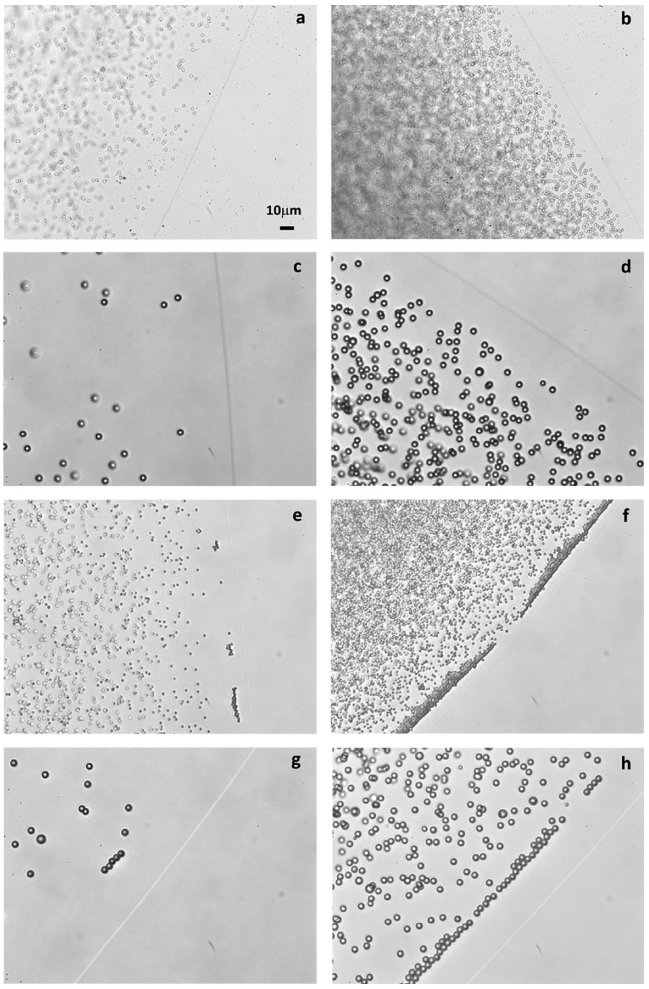

Figure 9. Particle distribution near the contact line observed under a microscope: (a) 0.5% 2 μm PS in silicone oil, (b) 5% 2 μm PS in silicone oil, (c) 0.5% 6 μm PS in silicone oil, (d) 5% 6 μm PS in silicone oil, (e) 0.5% 2 μm PS in glycerin, (f) 5% 2 μm PS in glycerin, (g) 0.5% 6 μm PS in glycerin, and (h) 5% 6 μm PS in glycerin.

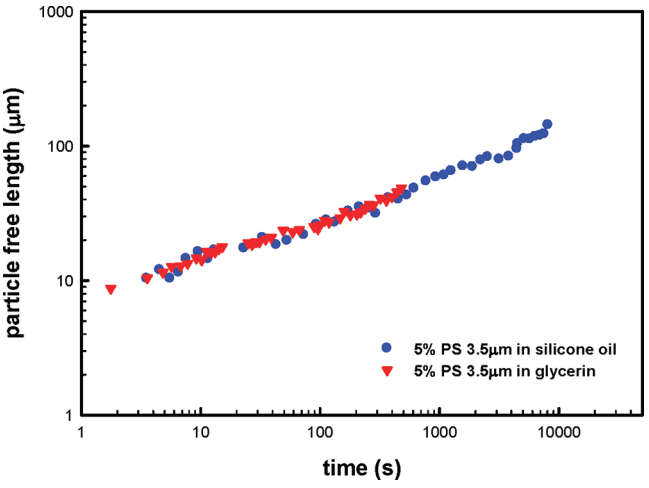

Figure 10. Particle-free region length vs time near the contact line.

is faster than that of the pure glycerin while no such phenomenon is observed in the case of silicone oil. It is predicted that particles that are completely wetted and heavier than the liquid cannot protrude from the liquid–air interface.[41] Therefore, PS particles which are heavier than and completely wetting silicone oil are fully immersed within silicone oil. (The contact angles of liquids on PS surfaces are listed in Table 2.)

Table 2. Contact Angles and Densities of Liquids on PS Surfaces

particle	density$_{particle}$ (g/cm^3)	liquid	density$_{liquid}$ (g/cm^3)	$\theta_{p\text{-}liq}$ (deg)
PS	1.05	water	0.997	84
		glycerin	1.261	78
		silicone oil	0.968	≈0
PMMA	1.18	water	0.997	49
		glycerin	1.261	37
		silicone oil	0.968	5–10

On the other hand, PS is lighter than glycerin and the contact angle is 78°; therefore, some particles placed near the air–liquid interface should protrude from the liquid surface, and the captured particles should play a role in the motion of glycerin suspension.

When fully wetting particles approach the contact line, they turn around near the contact line and they neither accumulate near the contact line nor form a chain structure along the contact line. Therefore, there is almost no direct effect of particles in the motion of the contact line. In the case of partially wetting particles, as particles move to the contact line, some of them are captured by the shallow layer of the fluid and the captured particles are coalesced in short chains by the capillary force, which has been extensively studied by Kralchevsky and Nagayama.[42] The capillary force is a long-range force, and therefore, freely moving particles located nearby are attracted to the almost immobile particles captured at the contact line region. A short chain can become the seed of a longer chain as illustrated by Sangani et al.[29] when there is an outward flow toward the contact line: More particles become members of the string by the capillary force one by one while lengthening the chain. It appears that the formation of such a string is a random process and this appears to be the large variation in the contact line speed of suspension compared with the pure liquid. When particles protrude from the air–liquid interface, the contact angle at the moving contact line becomes larger than the angle without particles. The larger contact angle will result in the faster motion.[29] The situation is illustrated in Figure 11. In the figure the contact point will move further with

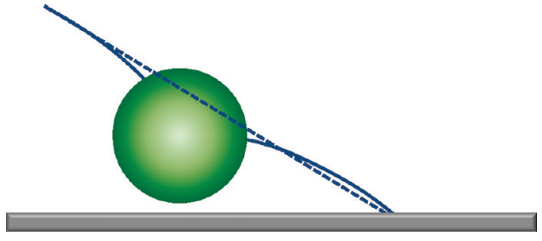

Figure 11. Deformation of the air–liquid interface and the increase in contact angle by the presence of a partially wetting particle near the moving contact line.

the presence of the particle while the larger contact angle is kept larger. The faster movement of the contact line is therefore the consequence of the change in the flow and surface shape at the intermediate region, the length scale of which is comparable with particle size. As particle loading becomes larger,

dx.doi.org/10.1021/la204256z | Langmuir 2012, 28, 2680–2689

the viscosity changes appreciably and the larger viscosity deters the movement of the contact line. In other words, the outer solution affects the intermediate solution. Also the drag force between the solid surface and hexagonal structure also deters the movement of the contact line. When particle loading is small, the particle alignment structure is not uniform along the contact line: A long chain, short chain, double chain, and even hexagonal structure can be seen. Depending on the particle arrangement the speed varies. When particle loading is 5%, particle arrangement looks much the same along the contact line. Therefore, the variation in contact line speed is smaller and hence the size of error bar is smaller.

The smaller density of particle is not a necessary condition for protruding and hence the alignment of particles. A PS suspension in water (the contact angle of water on PS surface is 84°, as shown in Table 2) also shows the similar behavior as the suspension in glycerin. The contact angle at the particle–liquid–air interface appears to be the dominant factor in forming the microstructure. When we performed the experiment with PMMA (polymethymethacrylate) particles, the arrangement of particles was relatively weak compared with PS suspensions. This result is consistent with the fact that the contact angle of glycerin on PMMA surface is smaller than that on PS.

Intermittency of Contact Line Motion. Even if the detailed motion of the contact line does not appear to cause the fundamental difference in contact line motions among different fluids, it will be worth considering in more detail. Figure 12 shows the detailed profiles of contact angle and contact line position relative to a fixed point for 1 s during spreading. The contact line positions of silicone oil and glycerin are not monotonically changing even if the positions were determined to subpixel levels. The contact line moves in a stop-and-go fashion, while it recedes slightly in some instances. The slight receding appears to be a numerical artifact that occurred during the estimation of the contact angle and contact line position. The problem of numerical artifacts will be considered later. The contact angle shows the decreasing trend while it increases slowly for a period of time and then decreases suddenly. Also when the contact angle decreases suddenly, the contact line jumps to a new position. The time scale of smooth motion is found to be less than 0.04 s (see below). This means that the contact line is held for a period and then it moves suddenly for less than $^{1}/_{500}$ s, the time interval between two subsequent image captures. This stop-and-go motion is observed regardless of the kind of liquid and the presence of particles. One may suspect that the stop-and-go motion could originate from numerical artifacts in determining the contact line position and contact angle, since the drop shape was determined by numerical fitting. To confirm whether it originated from such a problem, the contact line motion was examined using an inverted microscope. In this case the whole drop cannot be seen due to the limited window of the microscope at a high magnification and only the movement of the contact line can be traced for 1 s. Figure 13 also shows the changes in contact line positions of silicone oil and glycerin with and without particles (5%) for a short period with comparable contact line velocities. In this case, we did not determine the contact line position to a subpixel level since the pixel size under the microscope is 0.353 μm and is sufficiently small. As described above from the drop shape analysis, the contact line does not move continuously. They vary almost randomly with the maximum size of 0.04 s. If it moved continuously the length of the broken bars that

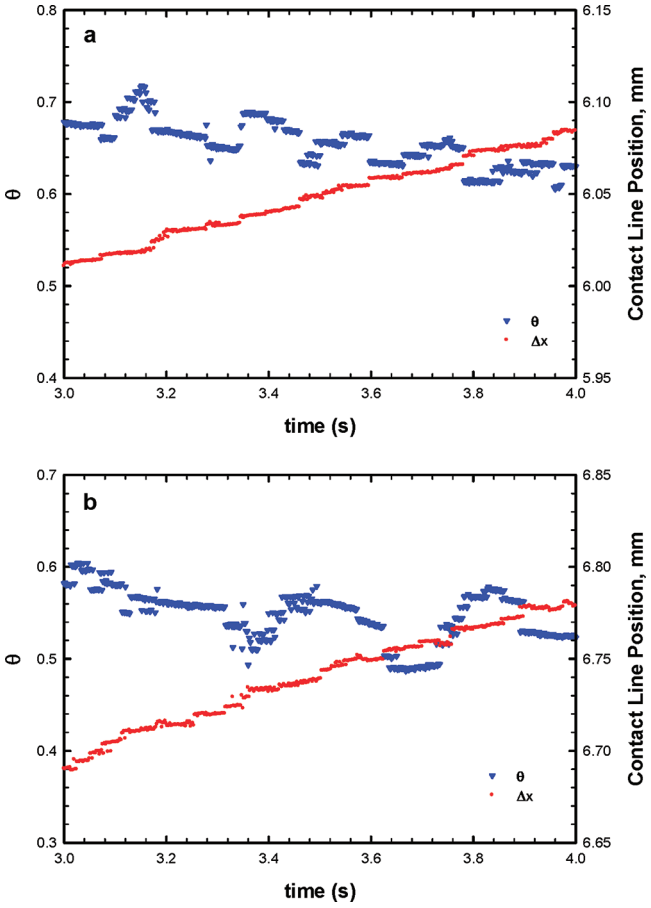

Figure 12. Intermittency of contact line motion of (a) silicone oil and (b) glycerin.

represent digitized positions should increase monotonically and continuously with time, considering that the contact line speed decreases with time. This confirms that the contact line moves in a stop-and-go fashion as described already, regardless of the presence of particles. In Figure 13b,d, we have plotted the distribution of the number of frames that gives the same digitized position. In each figure the distributions is virtually the same regardless of the presence of particles. This is expected, since there is a particle-free region even in the case of suspensions and the contact line moves without being affected by particles locally. The slight difference in distribution between silicone oil and glycerin appears to be caused by the large difference in surface tension. This set of data confirms that the stop-and-go motion originated from the nonperfectness of the surface. However, receding is not observed. It appears that the slight receding that occurs in the side view analysis should be a numerical artifact in determining the drop shape. Also the fluctuation is much smaller in the microscopic view. Therefore, the relatively large fluctuation appears to be amplified in determining the drop shape by the interpolation method.

The fluctuations in contact angle and contact line speed in the present research are not as large as those of Leiske et al.'s experiment on surfactant solution.[9] In their case, the unique stick-release phenomenon was caused by the surface shear elasticity. As stated in the Experiment Section, the average distance between surface defects has an order of 500 nm (see Figure 2). Then the time required to travel this length has on the order of 0.025 s when the contact line speed has the typical

dx.doi.org/10.1021/la204256z | Langmuir 2012, 28, 2680–2689

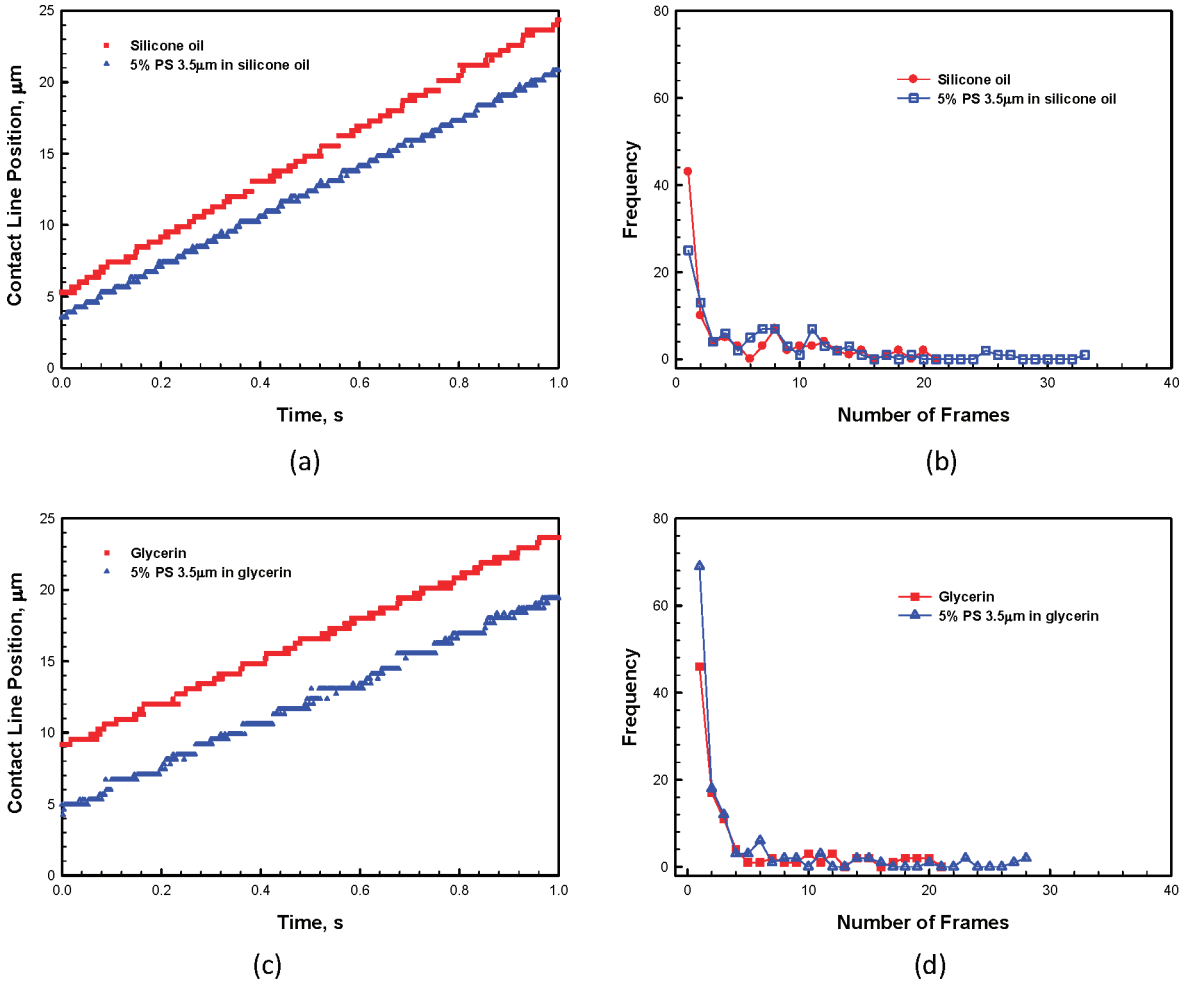

Figure 13. Changes in contact line positions with time and the distribution of the number of frames that gives the same digitized position: (a, b) silicone oil and (c, d) glycerin.

value of 20 μm/s. This time scale is consistent with the observed time scale of 0.04s for the smooth motion. Therefore, in the present case, the intermittent motion appears to be caused by the irregular characteristics of the solid surface. The independence of liquid on the motion also supports the argument that the motion is caused by the surface irregularity.

CONCLUSIONS

In this paper, we have considered the contact line motion of suspensions of PS particles of micrometer sizes. To determine the drop shape accurately, we judiciously used the drop image and its reflection and we traced the drop outline to the subpixel level. We investigated the contact line motion of silicone oil and glycerin without particles first to confirm that the Tanner–Voinov–Hoffman relation was valid. Then we showed that the relation was also valid for PS suspensions. The motion of the suspension in silicone oil did not show any noticeable change from that of pure fluid without particles. The motion of the suspension in glycerin, however, showed a noticeable difference compared with the motion of the pure fluid without particles. The difference between suspensions of silicone oil and glycerin was due to the microstructure change at the contact line region, and the microstructure change originated from the difference in wetting characteristics between two fluids. In the partially wetting glycerin, some particles protruded from the air–liquid interface, and these particles induced the capillary forces to become chained along the contact line and further packed into the hexagonal form. Other combinations such as PS in water and PMMA in glycerin confirmed that the difference in wetting behavior should be responsible for the microstructure development. In drying it has been thought that the alignment of particles along the contact line occurs when the contact line is pinned. But in the present research, we have found that the alignment occurs even during the spreading stage for the case of partially wetting particles. This means that the drying pattern can be different for suspensions of particles with different wetting characteristics. The contact line motions were found to be intermittent, regardless of the presence of particles. The motion is not regular and is stop-and-go fashioned. This irregular motion is found to be caused by the surface irregularities, which may be unavoidable as of now.

The present result on the contact line motion of suspensions can be used as the boundary condition at the contact line in numerical simulations on spreading of suspensions in various processes of printed electronics, inkjet printing, coating, and so on. Studies on more concentrated suspension are also needed to cover a wide range of particle loading.

ASSOCIATED CONTENT

Supporting Information

The microscopic observation of the particle motion of 5% suspension in silicone oil (video 1) and of the particle motion

dx.doi.org/10.1021/la204256z | *Langmuir* 2012, 28, 2680–2689

and microstructure formation of 5% suspension in glycerin (video 2). This material is available free of charge via the Internet at http://pubs.acs.org/.

AUTHOR INFORMATION

Corresponding Author

*E-mail: cykim@grtrkr.korea.ac.kr.

ACKNOWLEDGMENTS

This work was partially supported by Midcareer Researcher Program through NRF grant funded by the MEST (Ministry of Education, Science and Technology), Korea (No. 2010-0015186 and No. 2009-0079789)

REFERENCES

(1) Yarin, A. L. *Annu. Rev. Fluid Mech.* **2006**, *38*, 159−192.
(2) Son, Y.; Kim, C.; Yang, D. H.; Alm, D. J. *Langmuir* **2008**, *24*, 2900−2907.
(3) Ruschak, K. J. *Annu. Rev. Fluid Mech.* **1985**, *17*, 65−89.
(4) Weinstein, S. J.; Ruschak, K. J. *Annu. Rev. Fluid Mech.* **2004**, *36*, 29−53.
(5) Min, K. H.; Kim, C. *AIChE J.* **2010**, *56*, 2539−2550.
(6) Bergeron, V.; Bonn, D.; Martin, J. Y.; Vovelle, L. *Nature* **2000**, *405*, 772−775.
(7) Roux, D. C. D.; Cooper-White, J. J. *J. Colloid Interface Sci.* **2004**, *277*, 424−436.
(8) Bonn, D.; Eggers, J.; Indekeu, J.; Meunier, J.; Rolley, E. *Rev. Mod. Phys.* **2009**, *81*, 739−805.
(9) Leiske, D. L.; Monteux, C.; Senchyna, M.; Ketelson, H. A.; Fuller, G. G. *Soft Matter* **2011**, *7*, 7747−7753.
(10) Dussan, E. B. *Annu. Rev. Fluid Mech.* **1979**, *11*, 371−400.
(11) Degennes, P. G. *Rev. Mod. Phys.* **1985**, *57*, 827−863.
(12) Leger, L.; Joanny, J. F. *Rep. Prog. Phys.* **1992**, *55*, 431−486.
(13) Blake, T. D. *J. Colloid Interface Sci.* **2006**, *299*, 1−13.
(14) Ralston, J.; Popescu, M.; Sedev, R. *Annu. Rev. Mater. Res.* **2008**, *38*, 23−43.
(15) Wasan, D. T.; Nikolov, A. D. *Nature* **2003**, *423*, 156−159.
(16) Chengara, A.; Nikolov, A. D.; Wasan, D. T.; Trokhymchuk, A.; Henderson, D. J. *Colloid Interface Sci.* **2004**, *280*, 192−201.
(17) Chengara, A. V.; Nikolov, A. D.; Wasan, D. T. *Adv. Polym. Sci.* **2008**, *218*, 117−141.
(18) Nikolov, A.; Kondiparty, K.; Wasan, D. *Langmuir* **2010**, *26*, 7665−7670.
(19) Sefiane, K.; Skilling, J.; MacGillivray, J. *Adv. Colloid Interface Sci.* **2008**, *138*, 101−120.
(20) Kondiparty, K. K. K.; Nikolov, A.; Wu, S.; Wasan, D. *Langmuir* **2011**, *27*, 3324−3335.
(21) Rio, E.; Daerr, A.; Lequeux, F.; Limat, L. *Langmuir* **2006**, *22*, 3186−3191.
(22) Huh, C.; Scriven, L. *J. Colloid Interface Sci.* **1971**, *35*, 85−101.
(23) Dussan, E.; Davis, S. *J. Fluid Mech.* **1974**, *65*, 71−95.
(24) Hoang, A.; Kavehpour, H. P. *Phys. Rev. Lett.* **2011**, *106*, 254501.
(25) Hocking, L. *Q. J. Mech. Appl. Math.* **1983**, *36*, 55.
(26) Voinov, O. *Fluid Dyn.* **1976**, *11*, 714−721.
(27) Tanner, L. H. *J. Phys. D: Appl. Phys.* **1979**, *12*, 1473−1484.
(28) Hoffman, R. L. *J. Colloid Interface Sci.* **1975**, *50*, 228−241.
(29) Sangani, A. S.; Lu, C.; Su, K.; Schwarz, J. A. *Phys. Rev. E* **2009**, *80* (1), 011603.
(30) Lok, K. P.; Ober, C. K. *Can. J. Chem.* **1985**, *63*, 209−216.
(31) Ou, J. L.; Yang, J. K.; Chen, H. *Eur. Polym. J.* **2001**, *37*, 789−799.
(32) Semal, S.; Blake, T. D.; Geskin, V.; de Ruijter, M. J.; Castelein, G.; De Coninck, J. *Langmuir* **1999**, *15*, 8765−8770.
(33) Roques-Carmes, T.; Mathieu, V.; Gigante, A. *J. Colloid Interface Sci.* **2010**, *344*, 180−197.
(34) Pitas, I. *Digital Image Processing Algorithms*; Prentice Hall: New York, 1993; Chapter 5.
(35) Krause, S; Lu, Z. *J. Polym. Sci.* **1981**, *19*, 1925−1928.
(36) Hoyt, L. F. *Ind. Eng. Chem.* **1934**, *26*, 329−332.
(37) Ninomiya, N.; Yasuda, K. *J. Visualization* **2006**, *9*, 257−264.
(38) Cazabat, A. M.; Stuart, M. A. C. *J. Phys. Chem.* **1986**, *90*, 5845−5849.
(39) Ehrhard, P. *J. Fluid Mech.* **1993**, *257*, 463−483.
(40) Schiaffino, S.; Sonin, A. A. *Phys. Fluids* **1997**, *9*, 3172−3187.
(41) Rapacchietta, A. V.; Neumann, A. W. *J. Colloid Interface Sci.* **1977**, *59*, 555−567.
(42) Kralchevsky, P. A.; Nagayama, K. *Adv. Colloid Interface Sci.* **2000**, *85*, 145−192.